the Kir2.1 channels that underlie the inward rectifier potassium currents, I_{K1} (SQT3)[4]; *CACNA1C*, *CACNB2b*, and *CACNA2D1*, which encode the α1C, β2b, and α2δ-1-subunits of cardiac L-type calcium channels (SQT4, SQT5,[5] and SQT6[6]), respectively. SQT4 and SQT5 are considered clinical entities with the combined phenotypic characteristics of SQTS and Brugada syndrome, manifesting in a J point and ST-segment elevation in the right precordial ECG leads.

Regardless of the extensive genetic screening carried out on SQTS patients, genetic mutations have been identified in a small number of cases.[2–5,7,8] In 2005, Priori *et al.*[4] first reported that a *KCNJ2* mutation was responsible for SQTS (SQT3); however, no additional SQT3 variants have been reported thus far. This lack of progress has significantly hindered our advances in understanding the mechanisms underlying this disease. In the present study, we describe a novel *KCNJ2* mutation which impaired the inward rectification of Kir2.1 currents. This is a novel *KCNJ2* gain-of-function mechanism leading to SQTS.

2. Methods

2.1 Genetic analysis

Genetic analysis was performed after written informed consent in accordance with the study protocol approved by the Kyoto University ethical committee. The investigation conforms to the principles outlined in the Declaration of Helsinki. Genomic DNA was isolated from blood lymphocytes, and screened for the entire open-reading frames of *KCNQ1*, *KCNH2*, *KCNE1-3*, *KCNJ2*, *CACNA1C*, and *SCN5A* by denaturing high-performance liquid chromatography using a WAVE System Model 3500 (Transgenomic, Omaha, NE, USA). Abnormal conformers were amplified by polymerase chain reaction and sequencing was performed on an ABI PRISM 3100 Genetic Analyzer (Applied Biosystems, Foster City, CA, USA), and compared with 400 Japanese control alleles.

2.2 Neonatal rat ventricular myocyte isolation

This investigation was performed in accordance with the Guide for the Care and Use of Laboratory Animals, published by the National Institutes of Health (NIH Publication No. 85-23, revised 1996), and was approved by the Kyoto University Animal Experimentation Committee. A standard trypsin dissociation method was used to prepare neonatal rat ventricular myocytes (NRVMs).[9] The hearts were removed from 1- to 2-day-old Wistar rats euthanized by decapitation. The ventricles were minced, and the myocytes were dissociated with trypsin. Dispersed cells were preplated on 100 mm culture dishes for 1 h at 37°C in 5% CO_2 to remove fibroblasts. Non-attached, viable myocytes were collected, and placed on 35 mm culture dishes.

2.3 Mutagenesis and transient transfection of *KCNJ2* plasmids

The entire coding region of the *KCNJ2* was subcloned into the pCMS-EGFP vector (Clontech, Palo Alto, CA, USA) using methods previously described.[10] The mutation was introduced by site-directed mutagenesis using the QuikChange Mutagenesis Kit (Stratagene, La Jolla, CA, USA). We sequenced the entire plasmid to confirm the presence of the mutation and the absence of any unwanted variations. To assess the functional modulation of mutant channels, human embryonic kidney (HEK) 293 cells were transiently transfected with *KCNJ2* WT and/or mutant plasmids using FuGENE 6 (Roche, Indianapolis, IN, USA) as directed in the manufacturer's instructions. In order to investigate the mutant's effects on myocyte action potentials, plasmids were transfected 1 day after plating NRVMs, using Lipofectamine 2000 (Invitrogen, Carlsbad, CA, USA).[11]

2.4 Cell surface expression of *KCNJ2*

Immunofluorescence microscopy was used to detect the presence of KCNJ2 channels on the plasma membrane of HEK 293 cells. A haemagglutinin (HA) epitope (YPYDVPDYA) was introduced into the pCMS-EGFP-KCNJ2 [wild-type (WT) and mutant] construct between residues Ala-115 and Ser-116 (extracellular loop between TM1 and TM2).[10,12] HEK 293 cells were transfected with 1.0 μg of WT or mutant plasmids, or 0.5 μg of each WT and mutant plasmids to assess a heterozygous condition in 35 mm glass-bottom dishes. Two days later, the cells were fixed with 4% paraformaldehyde solution, and images were taken at ×40 magnification on an LSM 510 confocal microscope (Carl Zeiss, Jena, Germany).

2.5 Electrophysiological analysis

For voltage-clamp experiments, a total of 0.75 μg of WT and/or mutant *KCNJ2* plasmids were transfected in HEK 293 cells; 48–72 h after transfection, functional assays were conducted on GFP-positive cells by a conventional whole-cell configuration of patch-clamp techniques at 37°C, using an Axopatch 200A patch clamp amplifier and a Digidata 1322A digitizer (Axon Instruments, Foster City, CA, USA).[10] Pipettes were filled with a solution (in mM): 140 KCl, 2 $MgCl_2$, 1 EGTA, and 10 HEPES (pH 7.3 with KOH). The bath solution was composed of (in mM): 135 NaCl, 5 KCl, 1 $MgCl_2$, 10 glucose, and 10 HEPES (pH 7.4 with NaOH).

In order to record action potentials on NRVMs, 3 μg of WT, or a mixture of 1.5 μg WT and 1.5 μg mutant *KCNJ2* plasmids, were transfected; 48–72 h after transfection, functional assays were conducted on non-transfected or transfected cells that were recognized by their obvious green fluorescence, using a whole-cell patch-clamp technique at 37°C with the same devices. Action potentials were evoked by 2 ms supra-threshold current pulses at 10 Hz in a current-clamp mode. The pipette solution contained (in mM): KCl 140, $MgCl_2$ 1, MgATP 4, NaCl 10, and HEPES 10 (pH 7.2 with KOH). Tyrode solution contained (in mM): NaCl 140, KCl 4, $CaCl_2$ 2, $MgCl_2$ 1, HEPES 10, and glucose 10 (pH 7.4 with NaOH). Action potential duration (APD) was measured as the time from the overshoot to 90% repolarization (APD_{90}).

2.6 Statistics

All the data are shown as mean ± standard error of the mean. For mean value and comparisons between two sample groups, an unpaired Student's *t*-test was used to evaluate statistical significance. For comparisons between multiple groups, we applied a Steel–Dwass test. For either evaluation, a *P*-value <0.05 was considered significant.

3. Results

3.1 Clinical features

An 8-year-old girl with a markedly shortened QT interval (QT = 172 ms, QTc = 194 ms; *Figure 1A*) had been suffering from multiple disorders, such as severe mental retardation, abnormal proliferation of oesophageal blood vessels, epilepsy, and Kawasaki disease. Upon presentation during a routine check-up, her treating physician noticed an irregular heart rhythm. Her 12-lead ECG showed AF (*Figure 1B*), and she underwent external electrical cardioversion because intravenous infusion of procainamide (15 mg/kg) failed to recover sinus rhythm. The echocardiography revealed no significant abnormality. During further evaluation with right-heart catheterization, the Swan–Ganz catheter induced supra-ventricular tachycardia when it was inserted in the right atrium, and ventricular fibrillation occurred at the position of the right ventricular outflow tract, which suggested the presence of increased myocardial irritability.

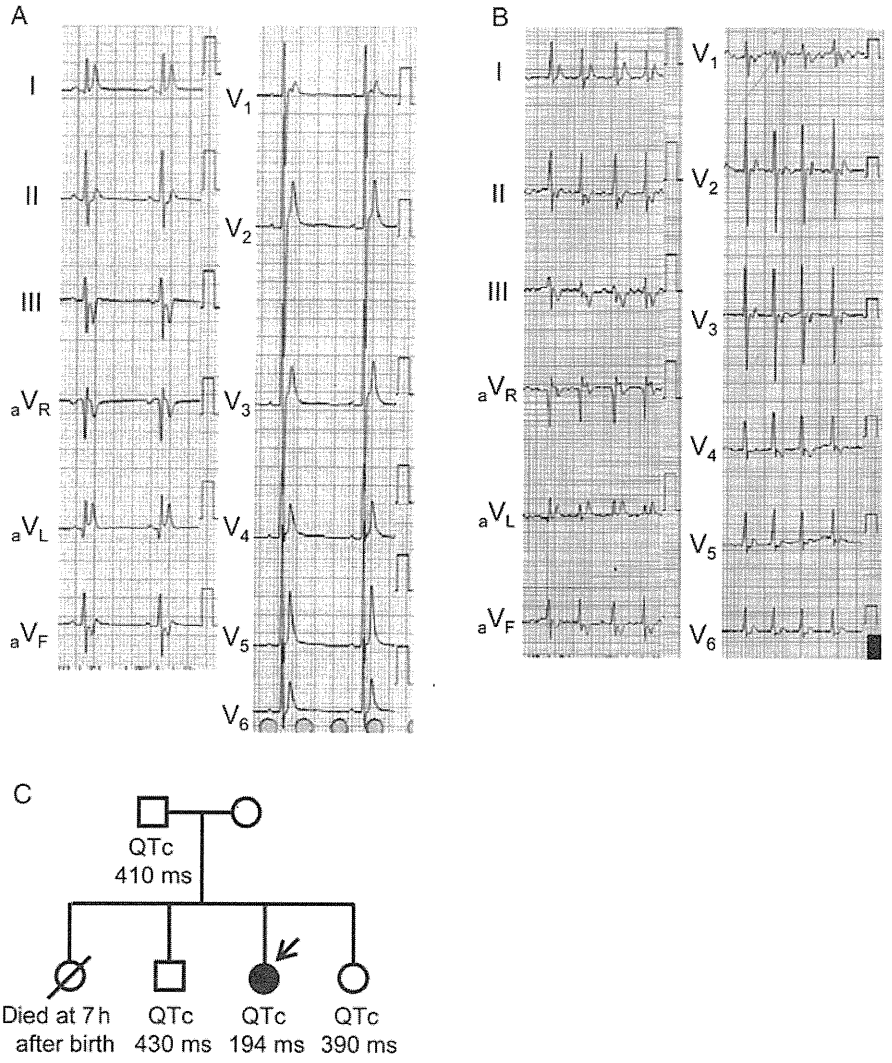

Figure 1 ECG of the proband and family pedigree. ECG shows sinus rhythm (*A*) and AF (*B*). The QT and QTc intervals were 172 and 194 ms, respectively. (*C*) Family pedigree. Arrow indicates the proband; a filled symbol indicates clinically and genetically affected individual.

She was diagnosed with SQTS from these clinical features (i.e. a markedly shortened QT interval, paroxysmal AF, and VF inducibility).

The proband had a family history of perinatal death in her elder sister (*Figure 1C*), but her family did not undergo genetic investigation or further clinical evaluation with the exception of ECGs taken for her father, elder brother, and younger sister. Genetic investigations could not be carried out due to a lack of informed consent. The ECGs for the family members displayed normal QTc intervals (410, 430, and 390 ms, respectively; *Figure 1C*).

3.2 Genetic analysis

In this patient, we screened for candidate cardiac ion channel genes (*KCNQ1*, *KCNH2*, *KCNE1-3*, *KCNJ2*, *CACNA1C*, and *SCN5A*). As a result of the genetic analysis, we identified a novel heterozygous mutation, a single-base substitution at nucleotide 902 (c.902T>A) in the *KCNJ2* gene, resulting in an amino acid change from methionine to lysine at 301 in the Kir2.1 potassium channel (*Figure 2A*). Met-301 is located in the C-terminal cytoplasmic domain of the channel (*Figure 2B*).[13] The amino acid at codon 301 (methionine) is highly conserved among different species (*Figure 2C*). Furthermore, this mutation was absent in 400 Japanese control alleles. We failed to identify mutations in any other candidate genes.

3.3 Cell surface expression of KCNJ2 mutants

In order to investigate whether the M301K mutations affect intracellular Kir2.1 trafficking, we introduced an HA epitope into the extracellular domain of KCNJ2, and examined the subcellular distribution of channels in transfected HEK 293 cells using confocal microscopy[10] (*Figure 2D*). *Figure 2D* illustrates the typical results of confocal imaging. HEK 293 cells were successfully transfected with either HA-*KCNJ2 WT*, *KCNJ2* WT/HA-M301K, or HA-M301K (*Figure 2D*, upper panels). All types of HA-tagged Kir2.1 proteins exhibited red fluorescence at the plasma membrane (*Figure 2D*, middle and lower panels), indicating that both homo- and heterozygous mutant channels were trafficking-competent.

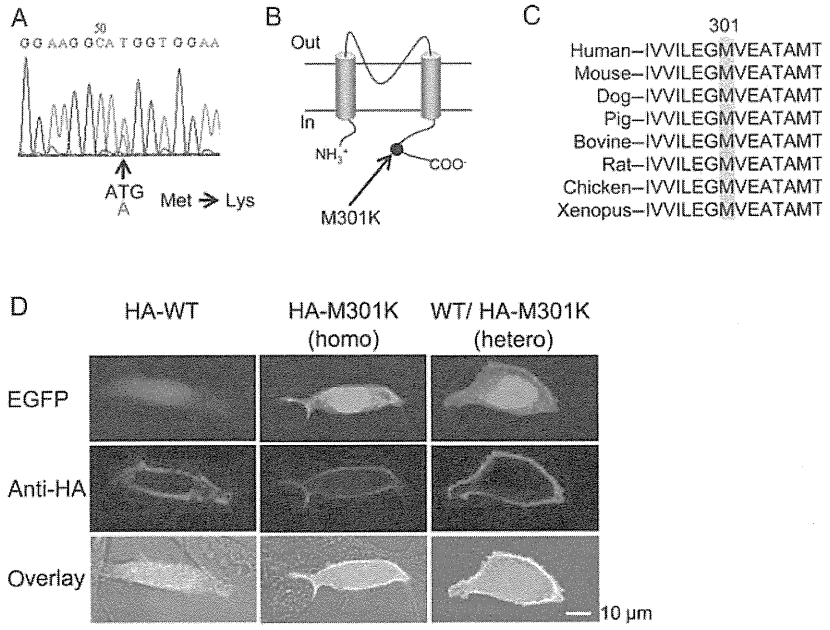

Figure 2 DNA sequence, topology, and homology. (*A*) Mutated DNA sequences derived from patient's genomic DNA. The trace shows a heterozygous substitution of thymine to adenine resulting in the amino acid change M301K. (*B*) Topology of the Kir2.1 channel showing localization of M301. (*C*) Amino acid sequence alignment of Kir2.1 channels from various species in the region surrounding codon 301 (highlighted). (*D*) Cellular localization of WT and mutant Kir2.1 channels. HA-WT indicates HA-tagged KCNJ2-WT, HA-M301K;HA-tagged KCNJ2-M301K, and WT/HA-M301K;KCNJ2-WT without HA-tagging and HA-tagged KCNJ2-M301K. The upper panel shows GFP, the middle panel shows the red fluorescence of the secondary anti-HA antibody, and the bottom panel is a mergence of the green fluorescence, red fluorescence, and transmission.

3.4 Cellular electrophysiology

We performed a functional characterization of the mutant channels in HEK 293 cells. *Figure 3A* shows representative current traces from cells expressing *KCNJ2* WT, M301K, or WT/M301K, elicited by voltage-clamp steps (duration 400 ms) from −120 to +100 mV (10 mV step), applied from a holding potential of −60 mV. The currents were normalized to cell capacitance and were plotted as a function of test potentials (*Figure 3B*). As previously reported, expression of the *KCNJ2* WT in HEK 293 cells resulted in normal inward rectifying potassium currents (*Figure 3A* left panel and blue symbols in *Figure 3B*). When M301K mutant channels were expressed alone, they were entirely non-functional (*Figure 3A* middle panel and green symbols in *Figure 3B*). In contrast, when cells were co-transfected with both equimolar WT and M301K, ample potassium currents showing a very weak inward rectification could be recorded (*Figure 3A* right panel and red symbols in *Figure 3B*). Average current densities were significantly smaller than those of WT Kir2.1 channels at potentials between −120 and −90 mV ($P < 0.05$), and significantly larger at potentials between −30 and +100 mV ($P < 0.05$).

3.5 Contribution of amino acid charge at residue 301 to Kir2.1 currents

Methionine at 301 is located within the G-loop that forms the narrowest segment of the cytoplasmic pathway,[13,14] and negatively charged amino acids on the inner wall of the cytoplasmic pore, where the G-loop is located, are known to be important for the strength of the inward rectification.[13–15] We therefore speculated that the amino acid charge at this position may be crucial for the inward rectification of Kir2.1 channels, and that its change from methionine (neutrally charged) to lysine (positively charged) may result in functional changes in Kir2.1 currents. In order to analyse the contribution of the amino acid charge at 301 to inward rectification, we changed the amino acid at M301 to another positively charged amino acid, arginine, and to another neutral amino acid, alanine, for comparison. *Figure 4A* illustrates the whole-cell Kir2.1 currents in homo- and heterozygous mutant conditions for M301R (left panel) and M301A (right panel). Homozygous M301R mutant channels displayed no functional currents, whereas WT/M301R attenuated the inward rectification (*Figure 4A* left panel). These observations suggest that the currents through the M301R channels are similar to those of the M301K channels (*Figure 3*) under both homo- and heterozygous conditions. On the other hand, in the M301A channels—in which the residual charge remained neutral—the currents showed normal inward rectification in both homo- and heterozygous conditions similar to those produced by WT Kir2.1 channels (*Figure 4A* right panel). In order to evaluate the intensity of inward rectifying properties, we assessed the rectification index, along with the ratio of the current amplitudes at 0 and −100 mV.[15] *Figure 4B* shows the rectification indexes obtained from WT, M301A (0.10 ± 0.02, $n = 10$), WT/M301A (0.073 ± 0.015, $n = 11$), WT/M301K (1.12 ± 0.16, $n = 11$), and WT/M301R (0.99 ± 0.14, $n = 11$). Although the rectification indexes for WT/301A and M301A showed no significant difference, the indexes for both WT/M301K and WT/M301R were significantly increased in comparison with WT (0.061 ± 0.01, $n = 15$, $P < 0.001$, left-most bar in *Figure 4B*).

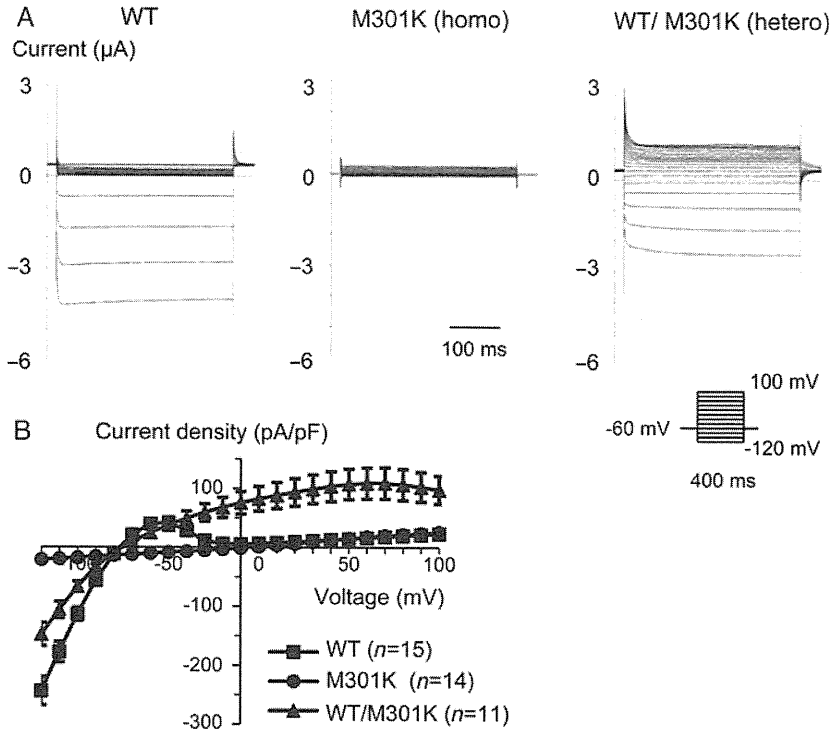

Figure 3 Voltage-clamp recordings from transfected HEK 293 cells. (*A*) Representative current traces of WT, M301K, and WT/M301K. Currents were elicited by 400 ms depolarizing voltage steps from −120 to +100 mV and from a holding potential of −60 mV. (*B*) Current–voltage relationships are plotted as the current. Current density was calculated by dividing the whole-cell current amplitude by cell capacitance. No functional currents were recorded in the homozygous M301K channels. On the other hand, the mean current densities of the WT/M301K channels are significantly larger than the WT ($P < 0.05$) at each voltage from −30 to +100 mV, and smaller at each voltage from −120 to −90 mV ($P < 0.05$).

3.6 Action potentials recording in *KCNJ2*-M301K-transfected NRVMs

We investigated the impacts of M301K mutant Kir2.1 channels on NRVMs' action potentials using a transient transfection method. *Figure 5A* shows typical action potentials recorded for non-transfected (control) NRVMs (*Figure 5A*, left panel), and NRVMs transfected with *KCNJ2* WT or WT/M301K (*Figure 5A* middle and right panels, respectively). Phase 3 repolarization was accelerated in the *KCNJ2* WT- and WT/M301K-overexpressed groups (*Figure 5A* middle and right panels, respectively) and we could further note that the dome is nearly lost in the WT/M301K group. APD_{90} was significantly abbreviated in the *KCNJ2* WT-overexpressed group (28.2 ± 3.4 ms, $n = 10$, $P < 0.001$, *Figure 5A*, middle panel) in comparison with the control group (123.3 ± 12.2 ms, $n = 11$, *Figure 5A*, left panel; bar graphs in *Figure 5B*). Additionally, APD90 was significantly shorter in the WT/M301K mutant-overexpressed group (9.4 ± 2.1 ms, $n = 16$, $P < 0.001$, *Figure 5A*, right panel; bar graph in *Figure 5B*) than in the WT-overexpressed group.

4. Discussion

4.1 Major findings

In the present study, we identified a novel heterozygous *KCNJ2* mutation, M301K, in a patient with a markedly shortened QT interval. The QT interval, 172 ms, of this patient is the shortest among previous SQTS reports,[2–7,16] to our knowledge. The methionine at position 301 is located in the C-terminus of Kir2.1 channel, and is considered to form a pore-facing loop region.[13] Functional assays using a heterologous expression system revealed that homozygous M301K Kir2.1 channels carried no currents with preserved plasma membrane expression; however, heterozygous WT/M301K Kir2.1 channels attenuated inward rectifying properties, which resulted in increased outward currents for positive voltages and negative voltages down to −30 mV. Significant increases in outward currents within the voltage range of the action potentials shortened APD by accelerating membrane repolarization as shown in *Figure 5*, which is implicated in increased cardiac vulnerability.

4.2 Impaired inward rectification of Kir2.1 currents: a novel mechanism predisposing SQTS

In 2005, Priori *et al.*[4] first reported a heterozygous gain-of-function *KCNJ2* mutation, D172N, in a patient with SQTS. In the report, homozygous D172N Kir2.1 channels displayed larger outward currents compared with WT Kir2.1 alone, and heterozygous channels yielded intermediate results. In both homozygous and heterozygous D172N mutant channels, the inward rectification properties of Kir2.1 currents were preserved. In heterozygous M301K mutant channels identified in our patient, however, the inward rectification was significantly reduced, allowing ample outward potassium currents at positive potentials. In addition, it should be emphasized that the homozygous M301K mutant channels were non-functional. These functional changes, such as the impaired inward rectification of the

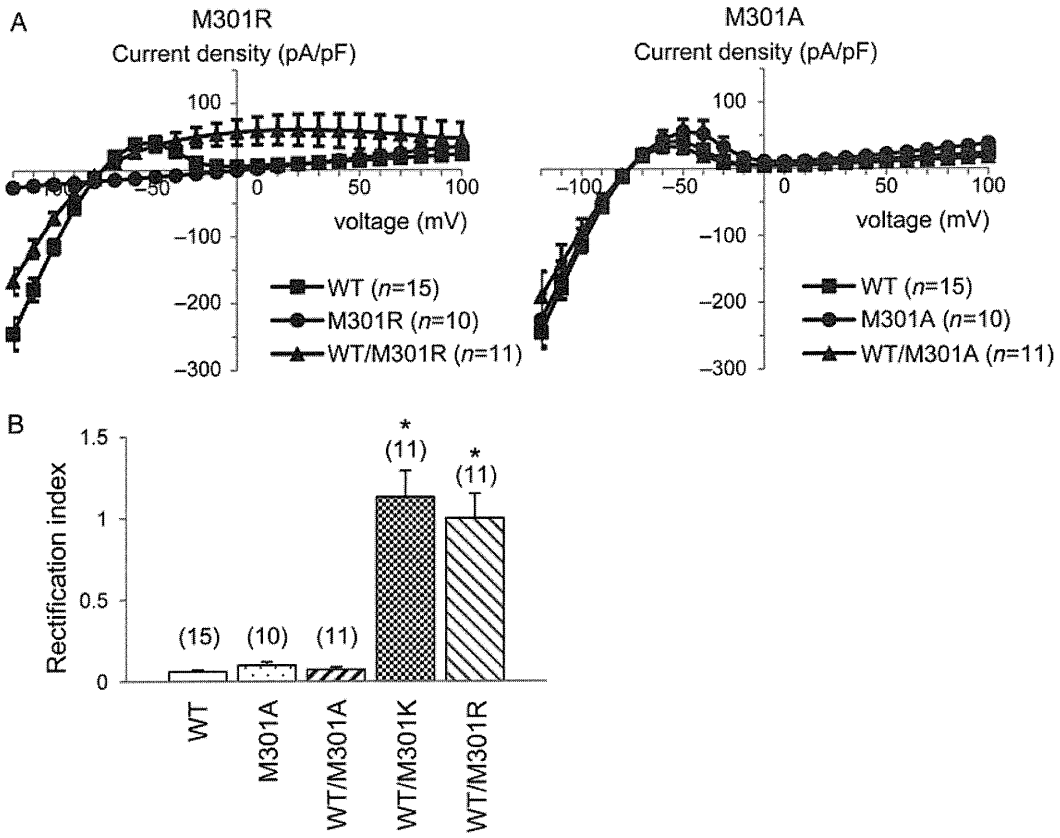

Figure 4 Comparison of macroscopic currents through WT Kir2.1 and mutants. (*A*) Current–voltage relationships for WT, M301R, and M301A are shown. M301R mutant channels displayed no functional currents and WT/M301R mutant channels displayed decreased inward rectification. On the other hand, the currents recorded in the homozygous M301A and heterozygous WT/M301A mutant channels showed no significant difference from WT. (*B*) Rectification index for WT ($n = 15$), M301A ($n = 10$), WT/M301A ($n = 11$), WT/M301K ($n = 11$), and WT/M301R ($n = 11$) channels. The rectification index was calculated by dividing the value of the outward currents measured at 0 mV by the absolute value of the inward currents measured at −100 mV. *$P < 0.001$.

Kir 2.1 currents resulting in increased outward currents, are a novel *KCNJ2* gain-of-function mechanism predisposing SQTS.

The phenotypic characteristics of our index patient somewhat differ from those of the *KCNJ2*-D172N mutation carriers.[4] No apparent arrhythmias were recorded with D172N mutation carriers. On the other hand, our M301K patient showed paroxysmal AF and multiple disorders. Additionally, mechanical stimulation by a Swan–Ganz catheter induced paroxysmal supraventricular tachycardia and VF. Moreover, the QTc interval in our patient was much shorter (QTc = 194 ms, *Figure 1*) than that of the D172N carriers (QTc = 315 and 320 ms).[4] Another gain-of-function *KCNJ2* mutation, V93I, was reported in a familial AF case.[17] Their functional analysis showed a similar result with D172N, but the affected members had normal QT intervals. These diverse clinical manifestations may be related to the extent and the different gain-of-function mechanisms of the Kir2.1 currents.

4.3 Relationship between impaired inward rectification and charged amino acid residues at 301

Kir currents exhibit strong inward rectification, which is thought to be due to pore blocking induced by multivalent ions from intracellular Mg^{2+}.[18–20] Channel blockade by physiological concentrations of Mg^{2+} is influenced by the electrostatic negativity within the cytoplasmic pore.[15] Negative charges on the inner wall of the cytoplasmic pore are therefore key determinants of the strength of the inward rectification. Many amino acid residues inside the pore demonstrate interactions with the ion over long distances, suggesting that mutations potentially affect ion or blocker energetics over the entire pore profile.[14,21] The M301K mutation causes the change of the amino acid residue at 301 from a non-charged amino acid residue, methionine, to a positively charged residue, lysine. In order to evaluate the importance of the charge at 301, additional whole-cell patch-clamp recordings were carried out on M301A (remained neutral) and M301R (neutral to positive) (*Figure 4*). Inward rectification of Kir2.1 currents was well preserved in both homozygous and heterozygous M301A channels. Heterozygous M301R channels, however, attenuated inward rectification, and homozygous M301R channels were non-functional similar to that of the M301K channels. These electrophysiological results indicate that the neutral amino acid residue at 301 plays an important role in generating Kir2.1 inward rectification. The decrease in the net negative charge within the cytoplasmic pore may facilitate the reduction in both the susceptibility of the channel to Mg^{2+} block and the voltage dependence of the blockade. It

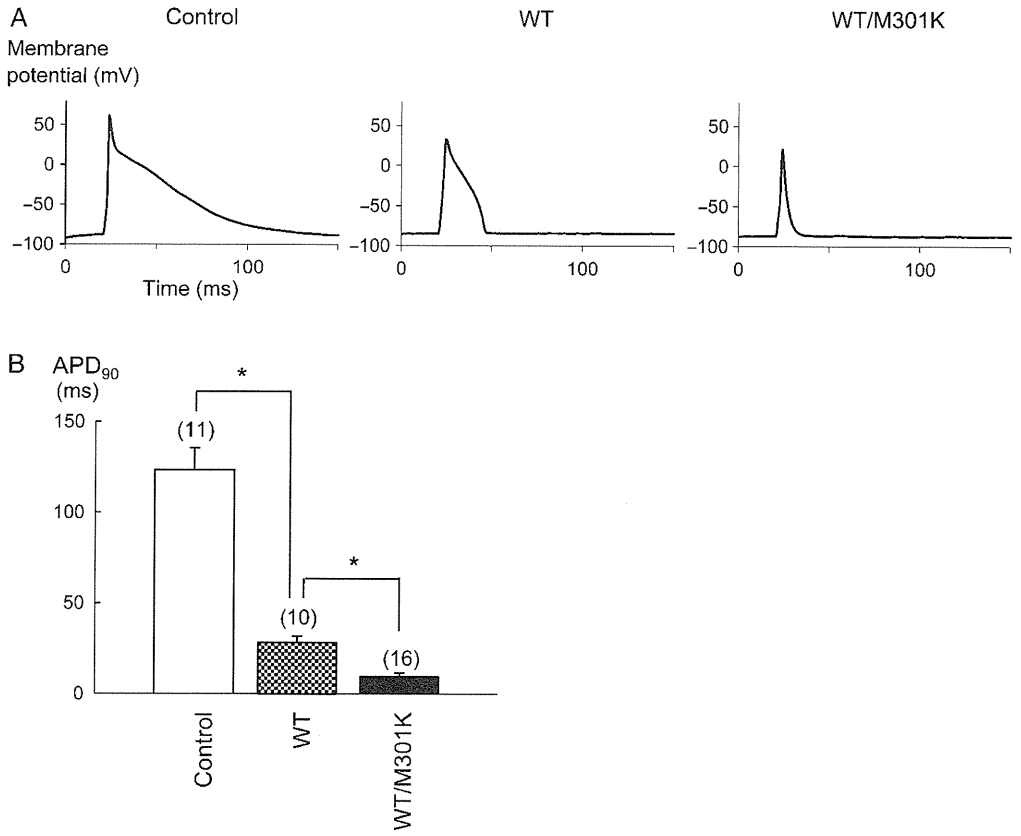

Figure 5 Effects of the M301K mutation on NRVM action potentials. Typical action potentials were demonstrated in a non-transfected cell (*A*), in a WT-overexpressed cell (*B*), and in a heterozygous overexpressed cell (*C*). Graphs show APD at 90% repolarization from the overshoot (*D*). In WT-overexpressed NRVMs, the plateau phase of the cardiac AP was markedly abbreviated, resulting in short repolarization. Under the heterozygous overexpressed condition, the results exhibited virtually no plateau phase, and the mean APD_{90} was significantly shorter in comparison with WT overexpressed alone. $^{*}P < 0.001$.

remains unknown why only tentative hetero-multimers of WT and M301K are active and lose their inward rectification properties. In homozygous M301K channels, all of the tetrameric subunits must have a positively charged lysine at 301, which may impair potassium ion permeation due to a conformational change in the near-pore region.

4.4 Heterozygous *KCNJ2*-WT/M301K overexpression shortened APD in NRVMs

In cardiomyocytes, Kir2.1, Kir2.2, and Kir2.3 channels are supposed to be able to co-assemble in order to modulate their channel properties.[22] Thus, there can be a multitude of Kir2.x heteromultimers, and to date a wide range of single-channel conductances of inward rectifier channels have been reported in studies conducted on various mammalian myocytes, including human.[23–25] This variety at the individual channel level may contribute to the different stoichiometry of the tetrameric channels.[26] Because Kir2.1 is a major component of IK1 in the myocardium, we overexpressed the *KCNJ2* M301K mutant channels in NRVMs to examine the effects of the mutation on APD. Overexpression with WT alone resulted in shorter APD in comparison with non-transfected myocytes (*Figure 5B*). These results are consistent with a previously published report.[27] Notably, heterozygous overexpression with WT and M301K further amplified the shortened APD (*Figure 5C*). These results were compatible with the electrophysiological changes assessed in HEK 293 cells, because the heterozygous WT/M301K channels showed a larger outward current than WT Kir2.1 channels under the physiological range of membrane potentials (*Figure 3*). Weak inward rectification observed in the heterozygous WT/M301K channels suggests that potassium ion can get through Kir2.1 channel at depolarized potential, probably resulting in loss of the action potential dome recorded in the *KCNJ2* WT/M301K-overexpressed group. The experiments were performed using a transient overexpression system that was different from the patient's heart, and the amount of overexpressed channels was difficult to be estimated accurately. But, these results are beneficial in understanding that the heterozygous *KCNJ2* M301K mutation could abbreviate APD and cause an extremely short-QT interval in the patient's ECG.

4.5 Clinical features of the index patient with *KCNJ2*-M301K

Regarding the clinical criteria for the diagnosis of SQTS, they have yet to be defined. However, we should consider SQTS in a patient presenting with a QTc <340 ms and other factors suggestive of arrhythmia (such as syncope or family history of sudden death).[28] A prominent clinical manifestation of SQTS is arrhythmias, such as AF

and VF.[1–5,7] In this patient, however, additional medical histories not limited to arrhythmias, such as severe mental retardation, abnormal proliferation of the oesophageal blood vessels, epilepsy, and Kawasaki' disease, were also documented. Because *KCNJ2* is known to be expressed in a variety of tissues, such as cardiac and skeletal muscle, the brain, arterial smooth muscle cells and developing bony structures of the craniofacial region, extremities, and vertebrae,[29–31] some of her compound disorders may be attributed to the *KCNJ2* mutation. In fact, loss-of-function mutations in *KCNJ2* cause Andersen–Tawil syndrome, which is characterized by prolonged repolarization, dysmorphic features, and periodic paralysis.[10,32] In the family of our female patient, we could not perform extensive genetic testing. We cannot exclude the possibility of the presence of other affected genes. Further analyses using knock-in mice or induced pluripotent stem cells would culminate monumental insight into the relationship between the *KCNJ2* M301K mutation and the patient's extra-cardiac phenotypes.

4.6 Conclusions

We described a novel *KCNJ2* gain-of-function mutation, M301K, in a patient with SQTS. Functional assays revealed no functional currents in the homozygous channels, whereas impaired inward rectification in the heterozygous channels manifested in larger outward currents, which is a novel mechanism predisposing SQTS.

Acknowledgements

We thank Dr Richard H. Kaszynski at the Kobe University School of Medicine for his critical reading of this manuscript.

Conflict of interest: none declared.

Funding

This work was supported by research grants from the Ministry of Education, Culture, Science, and Technology of Japan (T.M. and M.H.), the Takeda Science Foundation (T.M.), the Miyata Cardiac Research Promotion Foundation (T.M.), Japan Heart Foundation/Novartis Grant for Research Award on Molecular and Cellular Cardiology (T.M.), the Uehara Memorial Foundation (M.H.), Suzuken Memorial Foundation (T.K.), and health science research grants from the Ministry of Health, Labor, and Welfare of Japan for Clinical Research on Measures for Intractable Diseases (T.M. and M.H.).

References

1. Gussak I, Brugada P, Brugada J, Wright RS, Kopecky SL, Chaitman BR *et al.* Idiopathic short QT interval: a new clinical syndrome? *Cardiology* 2000;**94**:99–102.
2. Brugada R, Hong K, Dumaine R, Cordeiro J, Gaita F, Borggrefe M *et al.* Sudden death associated with short-QT syndrome linked to mutations in HERG. *Circulation* 2004; **109**:30–35.
3. Bellocq C, van Ginneken AC, Bezzina CR, Alders M, Escande D, Mannens MM *et al.* Mutation in the KCNQ1 gene leading to the short QT-interval syndrome. *Circulation* 2004;**109**:2394–2397.
4. Priori SG, Pandit SV, Rivolta I, Berenfeld O, Ronchetti E, Dhamoon A *et al.* A novel form of short QT syndrome (SQT3) is caused by a mutation in the KCNJ2 gene. *Circ Res* 2005;**96**:800–807.
5. Antzelevitch C, Pollevick GD, Cordeiro JM, Casis O, Sanguinetti MC, Aizawa Y *et al.* Loss-of-function mutations in the cardiac calcium channel underlie a new clinical entity characterized by ST-segment elevation, short QT intervals, and sudden cardiac death. *Circulation* 2007;**115**:442–449.
6. Templin C, Ghadri JR, Rougier JS, Baumer A, Kaplan V, Albesa M *et al.* Identification of a novel loss-of-function calcium channel gene mutation in short QT syndrome (SQTS6). *Eur Heart J* 2011;**32**:1077–1088.
7. Hong K, Piper DR, Diaz-Valdecantos A, Brugada J, Oliva A, Burashnikov E *et al.* De novo KCNQ1 mutation responsible for atrial fibrillation and short QT syndrome in utero. *Cardiovasc Res* 2005;**68**:433–440.
8. Garberoglio L, Giustetto C, Wolpert C, Gaita F. Is acquired short QT due to digitalis intoxication responsible for malignant ventricular arrhythmias? *J Electrocardiol* 2007; **40**:43–46.
9. Akao M, Ohler A, O'Rourke B, Marban E. Mitochondrial ATP-sensitive potassium channels inhibit apoptosis induced by oxidative stress in cardiac cells. *Circ Res* 2001; **88**:1267–1275.
10. Haruna Y, Kobori A, Makiyama T, Yoshida H, Akao M, Doi T *et al.* Genotype-phenotype correlations of KCNJ2 mutations in Japanese patients with Andersen-Tawil syndrome. *Hum Mutat* 2007;**28**:208.
11. Ma D, Tang XD, Rogers TB, Welling PA. An Andersen-Tawil syndrome mutation in Kir2.1 (V302M) alters the G-loop cytoplasmic K+ conduction pathway. *J Biol Chem* 2007;**282**:5781–5789.
12. Ballester LY, Benson DW, Wong B, Law IH, Mathews KD, Vanoye CG *et al.* Trafficking-competent and trafficking-defective KCNJ2 mutations in Andersen syndrome. *Hum Mutat* 2006;**27**:388.
13. Pegan S, Arrabit C, Zhou W, Kwiatkowski W, Collins A, Slesinger PA *et al.* Cytoplasmic domain structures of Kir2.1 and Kir3.1 show sites for modulating gating and rectification. *Nat Neurosci* 2005;**8**:279–287.
14. Tai K, Stansfeld PJ, Sansom MS. Ion-blocking sites of the Kir2.1 channel revealed by multiscale modeling. *Biochemistry* 2009;**48**:8758–8763.
15. Fujiwara Y, Kubo Y. Functional roles of charged amino acid residues on the wall of the cytoplasmic pore of Kir2.1. *J Gen Physiol* 2006;**127**:401–419.
16. Gollob MH, Redpath CJ, Roberts JD. The short QT syndrome: proposed diagnostic criteria. *J Am Coll Cardiol* 2011;**57**:802–812.
17. Xia M, Jin Q, Bendahhou S, He Y, Larroque MM, Chen Y *et al.* A Kir2.1 gain-of-function mutation underlies familial atrial fibrillation. *Biochem Biophys Res Commun* 2005;**332**:1012–1019.
18. Matsuda H, Saigusa A, Irisawa H. Ohmic conductance through the inwardly rectifying K channel and blocking by internal Mg2+. *Nature* 1987;**325**:156–159.
19. Horie M, Irisawa H, Noma A. Voltage-dependent magnesium block of adenosine-triphosphate-sensitive potassium channel in guinea-pig ventricular cells. *J Physiol* 1987;**387**:251–272.
20. Hille B. *Ion Channels of Excitable Membranes.* Sunderland: Sinauer Associates, 2001.
21. Robertson JL, Palmer LG, Roux B. Long-pore electrostatics in inward-rectifier potassium channels. *J Gen Physiol* 2008;**132**:613–632.
22. Liu Y, Fowler CD, Wang Z. Ontogeny of brain-derived neurotrophic factor gene expression in the forebrain of prairie and montane voles. *Brain Res Dev Brain Res* 2001; **127**:51–61.
23. Nakamura TY, Artman M, Rudy B, Coetzee WA. Inhibition of rat ventricular IK1 with antisense oligonucleotides targeted to Kir2.1 mRNA. *Am J Physiol* 1998;**274**: H892–H900.
24. Picones A, Keung E, Timpe LC. Unitary conductance variation in Kir2.1 and in cardiac inward rectifier potassium channels. *Biophys J* 2001;**81**:2035–2049.
25. Wible BA, De Biasi M, Majumder K, Taglialatela M, Brown AM. Cloning and functional expression of an inwardly rectifying K+ channel from human atrium. *Circ Res* 1995;**76**: 343–350.
26. Preisig-Muller R, Schlichthorl G, Goerge T, Heinen S, Bruggemann A, Rajan S *et al.* Heteromerization of Kir2.x potassium channels contributes to the phenotype of Andersen's syndrome. *Proc Natl Acad Sci USA* 2002;**99**:7774–7779.
27. Miake J, Marban E, Nuss HB. Functional role of inward rectifier current in heart probed by Kir2.1 overexpression and dominant-negative suppression. *J Clin Invest* 2003;**111**:1529–1536.
28. Viswanathan MN, Page RL. Short QT: when does it matter? *Circulation* 2007;**116**: 686–688.
29. Raab-Graham KF, Radeke CM, Vandenberg CA. Molecular cloning and expression of a human heart inward rectifier potassium channel. *Neuroreport* 1994;**5**:2501–2505.
30. Karkanis T, Li S, Pickering JG, Sims SM. Plasticity of KIR channels in human smooth muscle cells from internal thoracic artery. *Am J Physiol Heart Circ Physiol* 2003;**284**: H2325–H2334.
31. Karschin C, Karschin A. Ontogeny of gene expression of Kir channel subunits in the rat. *Mol Cell Neurosci* 1997;**10**:131–148.
32. Plaster NM, Tawil R, Tristani-Firouzi M, Canun S, Bendahhou S, Tsunoda A *et al.* Mutations in Kir2.1 cause the developmental and episodic electrical phenotypes of Andersen's syndrome. *Cell* 2001;**105**:511–519.

Distinct Characteristics of Circulating Vascular Endothelial Growth Factor-A and C Levels in Human Subjects

Hiromichi Wada[1]*, Shuichi Ura[1], Shuji Kitaoka[2], Noriko Satoh-Asahara[3], Takahiro Horie[4,5], Koh Ono[1,5], Tomohide Takaya[1,5], Rieko Takanabe-Mori[1], Masaharu Akao[1,6], Mitsuru Abe[1,6], Tatsuya Morimoto[1,7], Toshinori Murayama[4], Masayuki Yokode[4], Masatoshi Fujita[8], Akira Shimatsu[9], Koji Hasegawa[1]

1 Division of Translational Research, National Hospital Organization Kyoto Medical Center, Kyoto, Japan, **2** Health Evaluation Center, National Hospital Organization Kyoto Medical Center, Kyoto, Japan, **3** Division of Diabetic Research, National Hospital Organization Kyoto Medical Center, Kyoto, Japan, **4** Department of Clinical Innovative Medicine, Translational Research Center, Kyoto University Hospital, Kyoto, Japan, **5** Department of Cardiovascular Medicine, Graduate School of Medicine, Kyoto University, Kyoto, Japan, **6** Department of Cardiology, National Hospital Organization Kyoto Medical Center, Kyoto, Japan, **7** Division of Molecular Medicine, School of Pharmaceutical Sciences, University of Shizuoka, Shizuoka, Japan, **8** Department of Human Health Sciences, Graduate School of Medicine, Kyoto University, Kyoto, Japan, **9** Clinical Research Institute, National Hospital Organization Kyoto Medical Center, Kyoto, Japan

Abstract

The mechanisms that lead from obesity to atherosclerotic disease are not fully understood. Obesity involves angiogenesis in which vascular endothelial growth factor-A (VEGF-A) plays a key role. On the other hand, vascular endothelial growth factor-C (VEGF-C) plays a pivotal role in lymphangiogenesis. Circulating levels of VEGF-A and VEGF-C are elevated in sera from obese subjects. However, relationships of VEGF-C with atherosclerotic risk factors and atherosclerosis are unknown. We determined circulating levels of VEGF-A and VEGF-C in 423 consecutive subjects not receiving any drugs at the Health Evaluation Center. After adjusting for age and gender, VEGF-A levels were significantly and more strongly correlated with the body mass index (BMI) and waist circumference than VEGF-C. Conversely, VEGF-C levels were significantly and more closely correlated with metabolic (e.g., fasting plasma glucose, hemoglobin A1c, immunoreactive insulin, and the homeostasis model assessment of insulin resistance) and lipid parameters (e.g., triglycerides, total cholesterol (TC), low-density-lipoprotein cholesterol (LDL-C), and non-high-density-lipoprotein cholesterol (non-HDL-C)) than VEGF-A. Stepwise regression analyses revealed that independent determinants of VEGF-A were the BMI and age, whereas strong independent determinants of VEGF-C were age, triglycerides, and non-HDL-C. In apolipoprotein E-deficient mice fed a high-fat-diet (HFD) or normal chow (NC) for 16 weeks, levels of VEGF-A were not significantly different between the two groups. However, levels of VEGF-C were significantly higher in HFD mice with advanced atherosclerosis and marked hypercholesterolemia than NC mice. Furthermore, immunohistochemistry revealed that the expression of VEGF-C in atheromatous plaque of the aortic sinus was significantly intensified by feeding HFD compared to NC, while that of VEGF-A was not. In conclusion, these findings demonstrate that VEGF-C, rather than VEGF-A, is closely related to dyslipidemia and atherosclerosis.

Citation: Wada H, Ura S, Kitaoka S, Satoh-Asahara N, Horie T, et al. (2011) Distinct Characteristics of Circulating Vascular Endothelial Growth Factor-A and C Levels in Human Subjects. PLoS ONE 6(12): e29351. doi:10.1371/journal.pone.0029351

Editor: Marc Tjwa, University of Frankfurt-University Hospital Frankfurt, Germany

Received April 22, 2011; **Accepted** November 27, 2011; **Published** December 20, 2011

Funding: This work was supported in part by a Grant-in-Aid for Scientific Research from the Ministry of Education, Culture, Sports, Science and Technology of Japan, Japan Research Foundation for Clinical Pharmacology, and the Smoking Research Foundation (to HW). The funders had no role in study design, data collection and analysis, decision to publish, or preparation of the manuscript.

Competing Interests: The authors have declared that no competing interests exist.

* E-mail: hwada@kuhp.kyoto-u.ac.jp

Introduction

Obesity plays a major role in the development of dyslipidemia, hypertension and many other sub-clinical abnormalities that contribute to the atherosclerotic process and onset of cardiovascular events [1,2]. However, the mechanisms that lead from obesity to atherosclerosis and cardiovascular events are not fully understood.

It is widely accepted that adipose tissue development involves adipogenesis and angiogenesis [3]. Vascular endothelial growth factor-A (VEGF-A) signaling through VEGF receptor-2 (VEGFR-2) is the main angiogenic pathway [4]. It has been reported that VEGF-A accounts for much of the angiogenic activity of adipose tissue [5]. In addition, the administration of anti-VEGF-A antibody inhibited not only angiogenesis but also adipogenesis, which provides direct evidence that angiogenesis is essential for adipogenesis in obesity [6]. Circulating levels of VEGF-A are elevated in overweight and obese subjects [7]. Levels of VEGF-A is positively correlated with body mass index (BMI), and this correlation is apparently disconnected from insulin sensitivity [8]. However, a population-based cross-sectional study revealed that circulating VEGF-A levels have only a minor impact on the development of atherosclerosis [9].

Vascular endothelial growth factor-C (VEGF-C), a homologue of VEGF-A, plays a key role in lymphangiogenesis via VEGF receptor-3 (VEGFR-3). Deletion of *Vegfc* in mice leads to a complete absence of lymph vessels and embryonic lethality [10]. Overexpression of VEGF-C in the skin of transgenic mice induces

selective hyperplasia of the lymphatic vasculature [11]. In the clinical setting, serum levels of VEGF-C are increased in patients with some cancers and are suggested to be associated with lymph node and distant metastases, as well as a poor prognosis [12–16]. Serum levels of VEGF-C are also elevated in overweight and obese subjects [7]. However, precise relationships of serum VEGF-C levels with clinical, lipid, and metabolic profiles and atherosclerosis are unknown.

Therefore, in the present study, we examined: 1) circulating levels of VEGF-A and VEGF-C in subjects not receiving any medications and examined their association with clinical, lipid, and metabolic parameters in comparison with those of VEGF-A, and 2) serum levels of VEGF-A and VEGF-C as well as their expression levels in the aortic sinus including atheromatous plaque in apolipoprotein E (apoE)-deficient mice fed a high-fat-diet in comparison with those fed normal chow.

Methods

Subjects

A cross-sectional study was carried out during a specified period from April 2008 to March 2011. A total of 423 Japanese subjects not receiving any medications were recruited in the Health Evaluation Center of Kyoto Medical Center. All participants provided written informed consent. The study protocol was approved by the Institutional Ethics Committee of Kyoto Medical Center.

Data collection

Details are described elsewhere [17]. Briefly, blood was taken from the antecubital vein from 9 to 10 in the morning after a 12-h fast. Plasma levels of glucose and hemoglobin A1c (HbA1c), and serum levels of triglycerides, high-density-lipoprotein cholesterol (HDL-C), total cholesterol (TC), and low-density-lipoprotein cholesterol (LDL-C) were measured according to standard procedures. Non-high-density-lipoprotein cholesterol (nonHDL-C) was calculated employing the following formula: Non-HDL-C = TC−HDL-C. Immunoreactive insulin was measured using an enzyme immunoassay with a commercially available kit (Tosoh, Tokyo, Japan). The serum and plasma obtained were divided into aliquots and stored at −80°C until being assayed for VEGF-A and VEGF-C. Their serum (VEGF-C) or plasma (VEGF-A) concentrations were measured employing specific, commercially available, enzyme-linked immunosorbent assay (ELISA) kits according to the manufacturers' instructions (Quantikine, R&D Systems, Minneapolis, Minnesota, USA). The sensitivities of the assays for VEGF-C and VEGF-A were 4.6 and 5.0 pg/ml, respectively. Inter-/intra-assay coefficients of variation of ELISA for VEGF-C and VEGF-A were 7.2/3.5 and 7.0/4.5%, respectively. These assays were performed by an investigator blinded to the sources of the samples.

Experimental atherosclerosis

ApoE-deficient mice (129Ola × C57BL/6 mixed background) were a generous gift from Edward M. Rubin (University of California at Berkeley, Berkeley, California, USA) [18]. They were mated with C57BL/6 mice to produce F1 hybrids. The F1 apo E+/− mice were then backcrossed with C57BL/6 mice for 10 generations. Mice homogeneous for the apoE-null allele on a C57BL/6 background were subsequently generated. Male mice were used in the subsequent experiments. They were kept in a temperature-controlled facility under a 12-h light–dark cycle with free access to food and water. After being weaned at 4 weeks of age, mice were fed a normal chow diet (NC, Oriental Yeast Co., Ltd., Tokyo, Japan) until 6 weeks of age, when they were divided into an NC group and a high-fat-diet (HFD) group containing 40% fat and 0.15% cholesterol (Oriental Yeast). The experimental protocols were approved by the Ethics Committee for Animal Experiments of Kyoto University.

Serum samples from mice

At the age of 22 weeks, blood was drawn from the inferior vena cava of anesthetized mice and serum was separated by centrifugation at 4°C and stored at −80°C. Serum levels of total cholesterol, LDL-C, HDL-C, and triglycerides were measured using the standard methods (Nagahama Life Science Laboratory, Shiga, Japan). Those of VEGF-A and VEGF-C were measured employing specific ELISA kits according to the manufacturers' instructions (Quantikine, R&D Systems, Minneapolis, Minnesota, USA for VEGF-A, Cusabio Biotech Co., Ltd., Newark, Delaware, USA for VEGF-C).

Preparation of tissue and quantification of atherosclerosis in mice

After anesthesia, the mice were euthanized at 22 weeks of age, and their proximal aortas were excised, fixed in 4% paraformaldehyde (Nacalai Tesque, Inc, Kyoto, Japan), washed in sucrose, embedded in OCT compound (Tissue-Tek, Sakura Finetechnical Co., Ltd., Tokyo, Japan), frozen on dry ice, and then stored at −80°C until sectioning. The OCT-embedded aortas were sectioned with a cryostat, and 6-μm sections were obtained sequentially, beginning at the aortic valve. Eight sections obtained every 24 μm from the aortic sinus were stained with oil red O and used for quantification of the lesion areas. The total and atherosclerotic areas of each aorta were measured with image analysis (ImageJ), and the ratio of the atherosclerotic area to the total area was calculated.

Immunohistochemistry

The frozen sections were washed in phosphate-buffered saline (PBS) and endogenous peroxidase activity was blocked by 0.3% H_2O_2 in methyl alcohol for 30 min. The sections were washed in PBS (6 times, 5 each min) and mounted with 1% normal goat serum in PBS for 30 min. Subsequently, primary antibody (rat anti-mouse VEGF-A antibody (1:100), Biolegend, San Diego California, USA; rabbit anti-rat VEGF-C antibody (1:200) (also reacts with mouse and human VEGF-C), Abcam plc., Tokyo, Japan) was applied overnight at 4°C. After washing in PBS (6 times, 5 min), they were incubated with peroxidase-labeled secondary antibody polymer (Histofine Simple Stain Mouse MAX-PO (Rat or Rabbit), Nichirei Biosciences Inc., Tokyo, Japan) for 30 min. After washing in PBS (6 times, 5 min), a coloring reaction was carried out with diaminobenzidine (Wako Pure Chemical Industries, Osaka, Japan) and nuclei were counterstained with hematoxylin. The numbers of VEGF-A-positive and VEGF-C-positive cells were counted in a cross-section of the aortic sinus including atheromatous plaque in each mouse.

Statistical analysis

All statistical analyses were performed using Stat View version 5.0 for Windows (SAS Institute Inc., Cary, North Carolina, USA.). The Mann-Whitney U test was employed for comparisons of values between the two groups. Relationships between either of VEGF-A or VEGF-C and other parameters were analyzed by age- and gender-adjusted correlations and a stepwise linear regression. Stepwise regression was performed in a forward direction with F for the entry set to 4. Because triglycerides, fasting glucose,

immunoreactive insulin, homeostasis model assessment of insulin resistance (HOMA-IR), adiponectin, high-sensitivity C-reactive protein (hsCRP), and VEGF-A were normally distributed after logarithmic transformation, the logarithms of these parameters were used in the analyses. Data are expressed as the means ± SD or the medians and inter-quartile ranges, as appropriate. Values of $P<0.05$ were considered significant.

Results

Differential Association of Circulating Levels of VEGF-C and VEGF-A with Clinical, Lipid, and Metabolic Parameters

The clinical characteristics of subjects are shown in Table 1. The prevalence of obesity (defined as a body mass index >25 kg/m^2), hypertension (defined as systolic blood pressure >=140 or diastolic blood pressure >=90 mmHg), dyslipidemia (defined as LDL-C >=140 mg/dL, HDL-C<40 mg/dL, or triglycerides >=150 mg/dL) was 26, 13, and 42%, respectively. That of metabolic syndrome (defined as the presence of any 3 of the following 5 criteria: 1) increased waist circumference (>=85 cm in men or >=90 cm in women), 2) elevated triglycerides (>=150 mg/dL), 3) reduced concentration of high-density lipoprotein cholesterol (HDL-C) (<40 mg/dL in men or <50 mg/dL in women), 4) elevated blood pressure (systolic blood pressure >=130 or diastolic blood pressure >=85 mmHg), and 5) elevated fasting glucose (>=100 mg/dL)) was 16%. Thus, they were not necessarily healthy, but had yet to receive any medications. Distribution of circulating levels of VEGF-A were skewed, while levels of VEGF-C were almost normally distributed. Therefore, values of VEGF-A levels were log-transformed for subsequent analyses.

Table 1. Demographic Data of Human Subjects.

Number of patients, n	423
(Male/Female, n)	(281/142)
Age, y	45±9
Male gender,%	66±47
Body mass index, kg/m^2	22.9±3.1
Waist circumference, cm	83±9
Systolic blood pressure, mmHg	117±16
Diastolic blood pressure, mmHg	74±11
Fasting plasma glucose, mg/dL	95 [90–101]
Hemoglobin A1c,%	5.19±0.29
Immunoreactive insulin, mU/L	5.0 [4.0–8.0]
HOMA-IR	1.3 [0.8–1.8]
Triglycerides, mg/dL	96 [66–138]
HDL-C, mg/dL	69±18
Total cholesterol, mg/dL	209±32
LDL-C, mg/dL	126±31
Non-HDL-C, mg/dL	139±36
hsCRP, μg/mL	0.15 [0.10–0.30]
Adiponectin, μg/mL	7.7 [5.7–10.9]
VEGF-A, pg/mL	278 [163–434]
VEGF-C, pg/mL	6135±1409

Data are expressed as the mean ± SD, median [25–75 percentile], or number of patients. HDL-C: high-density lipoprotein cholesterol; LDL-C: low-density lipoprotein cholesterol; Non-HDL-C: non-high-density lipoprotein cholesterol; HOMA-IR: homeostasis model assessment of insulin resistance; hsCRP: high-sensitivity C-reactive protein; VEGF-A: vascular endothelial growth factor-A, VEGF-C: vascular endothelial growth factor-C.
doi:10.1371/journal.pone.0029351.t001

Then, we examined the association of circulating VEGF-A and VEGF-C levels with clinical, lipid, and metabolic parameters after adjusting for age and gender (Table 2). Levels of VEGF-A were significantly and more strongly correlated with the body mass index, waist circumference, and adiponectin levels than VEGF-C. Conversely, levels of VEGF-C were significantly and more closely correlated with lipid (e.g., triglyceride, TC, LDL-C, and non-HDL-C) and metabolic parameters (e.g., fasting plasma glucose, hemoglobin A1c, immunoreactive insulin, and HOMA-IR).

Independent Determinants of VEGF-A and VEGF-C levels

To identify independent determinants of VEGF-A and VEGF-C levels, stepwise multiple regression analyses were performed. The body mass index and age were independent determinants of VEGF-A levels (Table 3). In contrast, independent determinants of VEGF-C were age, triglycerides, non-HDL-C, and hemoglobin A1c (Table 3). These findings suggest that VEGF-A is associated with overweightness itself, whereas VEGF-C is closely associated with lipid and metabolic disorders. The correlation between VEGF-A and the body mass index and correlations of VEGF-C with triglycerides and non-HDL-C are shown in Figures 1A, B, and C, respectively.

Serum and expression levels in atheromatous plaque of VEGF-A and VEGF-C in apoE-deficient mice

To examine the relationship between VEGF-C and atherosclerosis with dyslipidemia, apoE-deficient mice, one of the most popular animal models of dyslipidemia and atherosclerosis, were fed a HFD (n=3) or NC (n=3) for 16 weeks. Thereafter, body weight (42±1 vs. 31±1 g, respectively, $P<0.05$) and serum levels of total cholesterol (1137±237 vs. 685±125 mg/dL, respectively, $P<0.05$) and LDL-C (393±78 vs. 162±21 mg/dL, respectively, $P<0.05$), but not HDL-C (28±5 vs. 20±3 mg/dL, respectively) and triglycerides (122±37 vs. 127±60 mg/dL, respectively), were significantly higher in the HFD than NC group. Atheromatous plaque in proximal aortas quantified by oil red O staining was markedly greater in the HFD than NC group (Figure 2A). Immunohistochemistry revealed that the number of VEGF-C-positive cells, but not that of VEGF-A, was significantly greater in HFD with advanced atherosclerosis than NC mice with minimal atherosclerosis (Figures 2B–F). Interestingly, serum levels of VEGF-C, but not those of VEGF-A, were significantly higher in HFD than NC mice (Figures 2G and H). These findings indicate that VEGF-C, rather than VEGF-A, is closely related to advanced atherosclerosis with marked hypercholesterolemia induced by HFD in apoE-deficient mice.

Discussion

The present study demonstrated that circulating levels of VEGF-C are closely associated with dyslipidemia in marked contrast to the fact that the strongest independent determinants of VEGF-A was the body mass index. These findings suggest that VEGF-A increases in association with overweightness itself; however, VEGF-C increases in association with dyslipidemia rather than overweightness per se. To our knowledge, this is the first study to report an association between VEGF-C and dyslipidemia.

Loebig et al. demonstrated that a positive correlation between VEGF-A and body mass index and that the relationship is

Table 2. Correlations of Vascular Endothelial Growth Factor-A (VEGF-A) and Vascular Endothelial Growth Factor–C (VEGF-C) with Other Parameters.

	VEGF-A		VEGF-C	
	r	*P*	*r*	*P*
Body mass index , kg/m^2	0.21	<0.0001	0.13	0.008
Waist circumference, cm	0.19	0.0001	0.13	0.007
Systolic blood pressure , mmHg	0.09	0.06	0.08	0.09
Diastolic blood pressure , mmHg	0.16	0.001	0.08	0.09
Fasting plasma glucose, mg/dL [a]	0.09	0.06	0.11	0.03
Hemoglobin A1c,%	0.11	0.02	0.13	0.007
Immunoreactive insulin, mU/L [a]	0.08	0.1	0.17	0.0006
HOMA-IR [a]	0.09	0.07	0.18	0.0003
Triglycerides, mg/dL [a]	0.10	0.04	0.23	<0.0001
HDL-C, mg/dL	−0.09	0.054	−0.08	0.1
Total cholesterol, mg/dL	0.07	0.2	0.18	0.0002
LDL-C, mg/dL	0.07	0.1	0.17	0.0004
Non-HDL-C, mg/dL	0.11	0.03	0.20	<0.0001
hsCRP, ng/mL [a]	0.10	0.04	0.12	0.01
Adiponectin, μg/mL [a]	−0.14	0.003	−0.08	0.1
VEGF-A, pg/mL [a]	-	-	0.11	0.03
VEGF-C, pg/mL	0.11	0.03	-	-

Abbreviations used in this table are the same as in Table 1.
[a]Log-transformed to obtain normal distributions. Values were adjusted for age and gender.
doi:10.1371/journal.pone.0029351.t002

apparently disconnected from insulin sensitivity [8]. Sandhofer et al. have shown that circulating VEGF-A levels have only a minor impact on the development of atherosclerosis [9]. However, VEGF-C is tightly associated with dyslipidemia, a potent risk factor as well as a therapeutic target of cardiovascular disease. In addition, we demonstrated that serum levels and expression levels in atheromatous plaque of VEGF-C, but not VEGF-A, were significantly increased in HFD-fed apoE-deficient mice with advanced atherosclerosis, suggesting that VEGF-C was more closely related to atherosclerosis with dyslipidemia than VEGF-A.

Table 3. Independent determinants of VEGF-A and VEGF-C levels.

	VEGF-A			VEGF-C		
	β	SEM	*F*	*β*	SEM	*F*
Body mass index, kg/m^2	0.16	3.4	11			
Age, y	0.11	0.1	5	−0.18	8.1	13.1
Triglycerides, mg/dL [a]				0.14	1.3	6.2
Non-HDL-C, mg/dL				0.14	2.2	5.7
Hemoglobin A1c, %				0.11	251	4.3

Abbreviations used in this table are the same as in Table 1. These models include data on the age, a male gender, body mass index, waist circumference, systolic and diastolic blood pressures, fasting plasma glucose, hemoglobin A1c, immunoreactive insulin, HOMA-IR, triglycerides, HDL-C, total cholesterol, LDL-C, non-HDL-C, hsCRP, and adiponectin.
doi:10.1371/journal.pone.0029351.t003

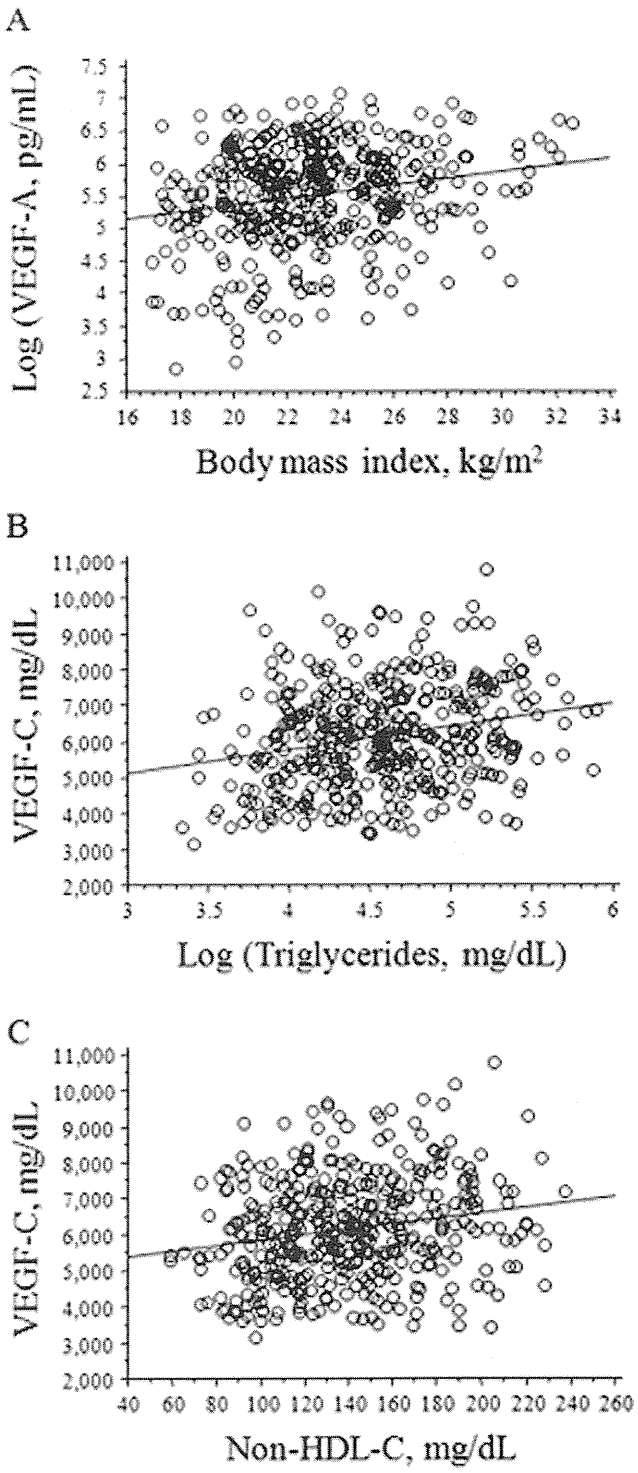

Figure 1. The correlation of circulating vascular endothelial growth factor-A (VEGF-A) or C (VEGF-C) levels with their independent determinants. A. The correlation between circulating VEGF-A levels and the body mass index. B. The correlation between those of VEGF-C and those of triglycerides. C. The correlation between those of VEGF-C and those of non-high-density-lipoprotein cholesterol (nonHDL-C).
doi:10.1371/journal.pone.0029351.g001

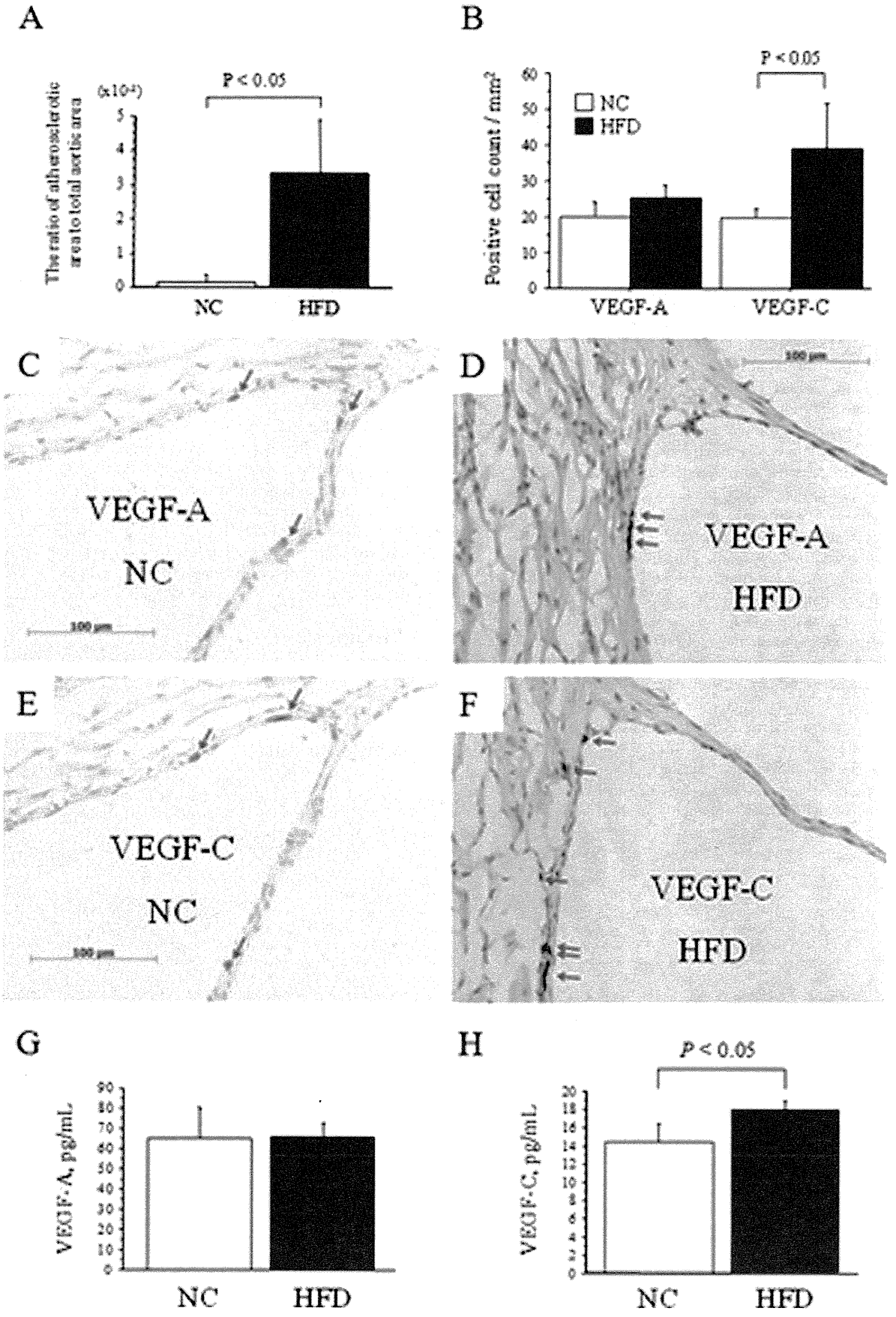
A
P < 0.05
(x10⁻²)
The ratio of atherosclerotic area to total aortic area
NC
HFD
B
P < 0.05
NC
HFD
Positive cell count / mm²
VEGF-A
VEGF-C
C
VEGF-A
NC
100 μm
D
100 μm
VEGF-A
HFD
E
VEGF-C
NC
100 μm
F
VEGF-C
HFD
G
VEGF-A, pg/mL
NC
HFD
H
P < 0.05
VEGF-C, pg/mL
NC
HFD

Figure 2. Serum and expression levels in atheromatous plaque of VEGF-A and VEGF-C in apoE-deficient mice. A. Quantification of the lesion size in the proximal aortas of apolipoprotein E (apoE)-deficient mice fed normal chow (NC, n = 3) or a high-fat-diet (HFD, n = 3). The ratio of the atherosclerotic area to the total area was significantly greater in HFD than NC mice. B. Quantification of the expression of vascular endothelial growth factor-A (VEGF-A) and vascular endothelial growth factor-C (VEGF-C) in NC and HFD mice. The expression of VEGF-C, but not VEGF-A, was significantly intensified by feeding HFD compared to NC. C–F. Representative microscopic views (x400) of the expression of VEGF-A in the aortic sinus of apoE-deficient mice fed NC (C) or a HFD (D), and those of VEGF-C in NC (E) or HFD (F) mice. The red arrows indicate VEGF-A- or VEGF-C-positive cells. G and H. Serum levels of VEGF-A (G) and VEGF-C (H) in apoE-deficient mice fed a HFD or NC for 16 weeks. The data are means ± SD.
doi:10.1371/journal.pone.0029351.g002

Therefore, VEGF-C might have more impact on atherosclerosis and future cardiovascular events than VEGF-A in humans.

VEGF-C induces lymphangiogenesis, which is involved in the draining of interstitial fluid and in immune function and inflammation [11]. It has been reported that VEGF-C levels are elevated in patients with refractory hypertension, and that VEGF-C/VEGFR-3 signaling in macrophages is a major determinant of the extracellular volume and blood pressure homeostasis [19]. The trapping of VEGF-C by soluble VEGF receptor-3 blocks VEGF-C signaling, and elevates the blood pressure in response to a high-salt-diet [19]. Thus, VEGF-C seems to be up-regulated to compensate for salt-diet-induced hypertension. Similarly, VEGF-C might be up-regulated to compensate for the development and progression of atheromatous plaque by draining lipid and/or inflammatory cells in response to dyslipidemia. However, further investigation is required regarding this matter.

While lymphatic vessels are rare in the atherosclerotic intima [20], membrane-bound VEGF receptor-2 (VEGFR-2) is up-regulated in atherosclerotic lesion in human coronary arteries [21]. A recent report suggested that a soluble form of VEGFR-2 (sVEGFR-2) inhibits lymphangiogenesis by blocking the VEGF-C function, and that the tissue-specific loss of the sVEGFR-2 gene induces lymphatic invasion of the normally alymphatic cornea and hyperplasia of skin lymphatics without affecting the blood vasculature [22]. These findings suggest that naturally occurring sVEGFR-2 acts as a molecular uncoupler of blood and lymphatic vessels [22]. We recently demonstrated that serum levels of sVEGFR-2 are increased in sera from subjects with metabolic syndrome in association with insulin resistance [17]. Thus, it is of interest to elucidate the interaction between VEGF-C and sVEGFR-2 in the regulation of lymphangiogenesis at vessel walls and in the progression of atherosclerosis.

Several study limitations should be considered. First, the present study was limited due to its moderate sample size. However, all the study participants did not receive any medications including statins or renin-angiotensin-system inhibitors, which could substantially affect serum levels of angiogenesis-related factors. Thus, the relationships between these biomarkers and established risk factors in this study are physiological. Second, this human study was cross-sectional, and, thus, the results cannot help answer the question of whether elevations of VEGF-C are merely consequences of metabolic abnormality or causes of future cardiovascular events in these subjects. Third, to elucidate its prognostic significance, the direct relationship of VEGF-C with cardiovascular events and/or atherosclerosis in patients should be investigated in future studies. Finally, at present, the sources of endogenous VEGF-C in human sera, and the relationships of their levels with cardiovascular lymphangiogenic activity are unclear.

Nevertheless, the present study first demonstrates that circulating levels of VEGF-C are closely associated with dyslipidemia and atherosclerosis. Future investigations are warranted to determine the precise role of lymphangiogenesis in the pathogenesis of atherosclerosis, and the clinical utility of serum VEGF-C levels.

Acknowledgments

We thank Akira Yamada, Yuko Iida, Haruhiko Eda, and Ryosuke Takeoka for technical assistance and Akemi Wada for technical and secretarial assistance.

Author Contributions

Conceived and designed the experiments: HW. Performed the experiments: SU SK NS TH TT RT . Analyzed the data: HW KH KO MA MA T. Morimoto MF AS. Contributed reagents/materials/analysis tools: T. Murayama MY. Wrote the paper: HW.

References

1. Must A, Spadano J, Coakley EH, Field AE, Colditz G, et al. (1999) The disease burden associated with overweight and obesity. JAMA 282: 1523–1529.
2. Abate N (2000) Obesity and cardiovascular disease. Pathogenetic role of the metabolic syndrome and therapeutic implications. J Diabetes Complications 14: 154–174.
3. Crandall DL, Hausman GJ, Kral JG (1997) A review of the microcirculation of adipose tissue: anatomic, metabolic, and angiogenic perspectives. Microcirculation 4: 211–232.
4. Lohela M, Bry M, Tammela T, Alitalo K (2009) VEGFs and receptors involved in angiogenesis versus lymphangiogenesis. Curr Opin Cell Biol 21: 154–165.
5. Hausman GJ, Richardson RL (2004) Adipose tissue angiogenesis. J Anim Sci 82: 925–934.
6. Nishimura S, Manabe I, Nagasaki M, Hosoya Y, Yamashita H, et al. (2007) Adipogenesis in obesity requires close interplay between differentiating adipocytes, stromal cells, and blood vessels. Diabetes 56: 1517–1526.
7. Silha JV, Krsek M, Sucharda P, Murphy LJ (2005) Angiogenic factors are elevated in overweight and obese individuals. Int J Obes (Lond) 29: 1308–1314.
8. Loebig M, Klement J, Schmoller A, Betz S, Heuck N, et al. (2010) Evidence for a relationship between VEGF and BMI independent of insulin sensitivity by glucose clamp procedure in a homogenous group healthy young men. PLoS One 5: e12610.
9. Sandhofer A, Tatarczyk T, Kirchmair R, Iglseder B, Paulweber B, et al. (2009) Are plasma VEGF and its soluble receptor sFlt-1 atherogenic risk factors? Cross-sectional data from the SAPHIR study. Atherosclerosis 206: 265–269.
10. Karkkainen MJ, Haiko P, Sainio K, Partanen J, Taipale J, et al. (2004) Vascular endothelial growth factor C is required for sprouting of the first lymphatic vessels from embryonic veins. Nat Immunol 5: 74–80.
11. Jeltsch M, Kaipainen A, Joukov V, Meng X, Lakso M, et al. (1997) Hyperplasia of lymphatic vessels in VEGF-C transgenic mice. Science 276: 1423–1425.
12. Tamura M, Ohta Y (2003) Serum vascular endothelial growth factor-C level in patients with primary nonsmall cell lung carcinoma: a possible diagnostic tool for lymph node metastasis. Cancer 9: 1217–1222.
13. Tamura M, Oda M, Tsunezuka Y, Matsumoto I, Kawakami K, et al. (2004) Chest CT and serum vascular endothelial growth factor-C level to diagnose lymph node metastasis in patients with primary non-small cell lung cancer. Chest 126: 342–346.
14. Mitsuhashi A, Suzuka K, Yamazawa K, Matsui H, Seki K, et al. (2005) Serum vascular endothelial growth factor (VEGF) and VEGF-C levels as tumor markers in patients with cervical carcinoma. Cancer 103: 724–730.
15. Wang TB, Deng MH, Qiu WS, Dong WG (2007) Association of serum vascular endothelial growth factor-C and lymphatic vessel density with lymph node metastasis and prognosis of patients with gastric cancer. World J Gastroenterol 13: 1794–1797.
16. Mouawad R, Spano JP, Comperat E, Capron F, Khayat D (2009) Tumoural expression and circulating level of VEGFR-3 (Flt-4) in metastatic melanoma patients: correlation with clinical parameters and outcome. Eur J Cancer 45: 1407–1414.
17. Wada H, Satoh N, Kitaoka S, Ono K, Morimoto T, et al. (2010) Soluble VEGF receptor-2 is increased in sera of subjects with metabolic syndrome in association with insulin resistance. Atherosclerosis 208: 512–517.
18. Plump AS, Smith JD, Hayek T, Aalto-Setälä K, Walsh A et al (1992) Severe hypercholesterolemia and atherosclerosis in apolipoprotein E-deficient mice created by homologous recombination in ES cells. Cell 71: 343–353.
19. Machnik A, Neuhofer W, Jantsch J, Dahlmann A, Tammela T, et al. (2009) Macrophages regulate salt-dependent volume and blood pressure by a vascular

endothelial growth factor-C-dependent buffering mechanism. Nat Med 15: 545–552.
20. Nakano T, Nakashima Y, Yonemitsu Y, Sumiyoshi S, Chen YX, et al. (2005) Angiogenesis and lymphangiogenesis and expression of lymphangiogenic factors in the atherosclerotic intima of human coronary arteries. Hum Pathol 36: 330–340.
21. Inoue M, Itoh H, Ueda M, Naruko T, Kojima A, et al. (1998) Vascular endothelial growth factor (VEGF) expression in human coronary atherosclerotic lesions: possible pathophysiological significance of VEGF in progression of atherosclerosis. Circulation 98: 2108–2116.
22. Albuquerque RJ, Hayashi T, Cho WG, Kleinman ME, Dridi S, et al. (2009) Alternatively spliced vascular endothelial growth factor receptor-2 is an essential endogenous inhibitor of lymphatic vessel growth. Nat Med 15: 993–994.

Am J Transl Res 2012;4(1):52-59
www.ajtr.org /ISSN:1943-8141/AJTR1110002

Original Article

An exploratory clinical trial for combination wound therapy with a novel medical matrix and fibroblast growth factor in patients with chronic skin ulcers: a study protocol

Naoki Morimoto[1], Kenichi Yoshimura[2], Miyuki Niimi[2], Tatsuya Ito[3], Harue Tada[2], Satoshi Teramukai[2], Toshinori Murayama[4], Chikako Toyooka[4], Satoru Takemoto[1], Katsuya Kawai[1], Masayuki Yokode[4], Akira Shimizu[3], Shigehiko Suzuki[1]

[1]Department of Plastic and Reconstructive surgery, Graduate School of Medicine, Kyoto University; [2]Department of Clinical Trial Design and Management, Translational Research Center, Kyoto University Hospital; [3]Department of Experimental Therapeutics, Translational Research Center, Kyoto University Hospital; [4]Department of Clinical Innovative Medicine, Translational Research Center, Kyoto University Hospital, Japan.

Received October 17, 2011; accepted November 20, 2011; Epub January 5, 2012; Published January 15, 2012

Abstract: Background: Chronic skin ulcers such as diabetic ulcers and venous leg ulcers are increasing and are a costly problem in health care. We have developed a novel artificial dermis, collagen/gelatin sponge (CGS), that is capable of the sustained release of basic fibroblast growth factor (bFGF) for more than 10 days. The objective of this study was to investigate the safety and efficacy of CGS impregnated with bFGF in the treatment of chronic skin ulcers. Methods/Design: Seventeen patients (≥ 20 years of age) with chronic skin ulcers that have not healed by conventional therapy for at least 4 weeks are being recruited. Patients will be applied with CGS impregnated with bFGF of 7 μg/cm^2 or 14 μg/cm^2 after debridement, and the wound bed improvement will be assessed 14 days after application. "Wound bed improvement" is defined as a granulated and epithelialized area on Day 14 in proportion to the baseline wound area after debridement of 50% or higher. Patients will be followed up until 28 days after application to observe the adverse events related to the application of CGS. Conclusion: This study has been designed to address the safety and efficacy of CGS impregnated with bFGF. If successful, this intervention may be an alternative to bioengineered skin substitutes and lead to substantial and important changes in the management of chronic skin ulcers such as diabetic ulcers and venous ulcers.

Keywords: Artificial dermis, basic fibroblast growth factor, skin ulcers, sustained release

Introduction

Non-healing or chronic skin ulcers are an increasing and costly problem in health care [1-4]. Chronic skin ulcers are caused by diabetes mellitus, venous insufficiency, pressure sores, collagen disease, trauma, or radiation. With the development of tissue engineering and advances in cell and molecular biology, novel bioengineered skin substitutes and genetically derived growth factors offer promise in the treatment of chronic skin ulcers [5-7]; however, there are still issues that remain to be solved in the treatment of those ulcers. Diabetic foot ulcers and venous leg ulcers are frequent and costly complications of their underlying diseases. The prevalence of foot ulcers ranges from 4% to 10% among persons diagnosed with diabetes mellitus [3, 4] and the annual population-based incidence of 1.0% to 5% [1, 3, 4], and the lifetime incidence may be as high as 25% [3, 4]. More than 15% of all ulcers result in some form of amputation [3, 4]. According to a previous report, venous leg ulcers recurred in 72% of cases and skin ulcers from other causes recurred in 45% of cases [2], and another report described recurrence in 48% of cases one year after skin grafting [8].

We developed a bilayered acellular artificial dermis composed of an upper silicone sheet and a lower collagen sponge [9, 10] by modifying the material described by Yannas and Burke [11, 12]. Artificial dermis has been used in the treatment of full-thickness skin defects resulting

from burns, trauma injuries and tumor removal. After application of the artificial dermis to skin defects, fibroblasts and capillaries penetrate and proliferate in the collagen sponge and dermis-like tissue is formed after degradation of the collagen sponge [9-11]. However, it is difficult to apply ordinary artificial dermis to chronic skin ulcers, because the artificial dermis has no resistance to infection and is easily infected before the infiltration of capillaries into the inner collagen sponge.

Basic fibroblast growth factor (bFGF), which was identified in 1974, promotes the proliferation of fibroblasts and capillary formation and accelerates tissue regeneration [13, 14]. In Japan, human recombinant bFGF (FIBRAST SPRAY; Kaken Pharmaceutical, Tokyo, Japan) has been used clinically for chronic skin ulcers since 2001, and its clinical effectiveness has been demonstrated [7, 15]. Recently, combination therapy involving bFGF and artificial dermis has been reported to accelerate dermis-like tissue formation in the treatment of traumatic wounds [16]. In addition, this combination therapy was reported to be effective for chronic skin ulcers such as diabetic foot ulcers, ulcers caused by collagen disease, oral steroids and arteriosclerosis obliterans [17-19]. This is because bFGF causes the proliferation of fibroblasts and strongly promotes angiogenesis in artificial dermis, leading to the early formation of dermis-like tissue and promoting wound healing; however, this combination therapy has not become the standard treatment of chronic ulcers, because once daily topical administration of bFGF is required to achieve the expected effect because the artificial dermis has no ability to retain bFGF and it rapidly diffuses away from the applied site and is also inactivated quickly after its administration in vivo; thus, significant burdens are imposed on both medical staff and patients for daily application. For these reasons, we have developed a novel artificial dermis, collagen/gelatin sponge (CGS), containing a 10wt% concentration of acidic gelatin that is capable of the sustained release of positively charged growth factors such as bFGF for more than 10 days in vivo [20]. In our previous study, CGS was used as a scaffold for dermal regeneration, the same as conventional artificial dermis, and degraded after application to the wound site, being replaced by dermis-like tissue [20].

In our previous studies to apply CGSs impregnated with 7 μg/cm^2 or 14 μg/cm^2 of bFGF to full-thickness skin defects of normal mice and decubitus created on diabetic mice, the time required for regeneration of dermis-like tissue in mice treated with CGSs with bFGF was half to one third of the time required in mice treated with conventional artificial dermis alone [21]. In another study using mucosal defects of dog palates, CGSs impregnated with 7 μg/cm^2 bFGF accelerated the regeneration of palatal mucosa with good neovascularization and showed less contracture [22]. Alternative therapies for chronic skin ulcers have been proposed, such as tissue engineering products, growth factors, and hyperbaric oxygen therapy [23, 24]. Hyperbaric oxygen therapy is a systemic therapy; therefore, it can be combined with CGSs. The mechanism of action of tissue engineering products is considered mainly as the effects of cytokines and growth factors secreted by living cells [25]. Our CGS impregnated with bFGF can sustain and release bFGF in a controlled manner; therefore, the effectiveness of CGS will either equal or surpass and be competitive in cost to tissue engineering products. Moreover, both CGS and bFGF can be stored at room temperature and used whenever needed. Usually, growth factors must be applied once or twice a day because of their rapid inactivation after administration, and CGS with bFGF will be superior in this respect.

In view of the above, combination therapy with this novel collagen-based artificial dermis (CGS) and bFGF is anticipated to be comparably minimally invasive and effective to tissue engineering products to promote wound healing even in patients with chronic skin ulcers. Thus, we propose to investigate the safety and efficacy of this combination therapy in the treatment of chronic skin ulcers.

Materials and methods

Primary objective

The objective of this study is to evaluate the safety and efficacy of CGS impregnated with bFGF in the treatment of chronic skin ulcers that are not expected to heal with conventional treatments.

Methods and design

Open-label, randomized, multiple dose, con-

trolled clinical trial.

Design

Two groups, a low-dose and high-dose bFGF group, have been set (**Figure 1**). In the initial step (Step 1), three patients will be enrolled in the low-dose group. After confirming the safety in the low-dose group, patients will be randomized to the low-dose or high-dose bFGF group in Step 2. Randomization-based comparison between dose groups can achieve significant improvements in accuracy and lack of bias. This comparison can provide useful information for designing and conducting future trials.

Setting and participants

This study is being conducted at Kyoto University Hospital. Patients with chronic skin ulcers are referred by physicians and also identified through a number of wound care clinics in Kyoto Prefecture and surrounding prefectures.

Inclusion criteria

1). Patients aged 20 years or older at informed consent. 2). Presence of chronic skin ulcers as below: not healing for at least 4 weeks with conventional treatments; skin graft is not expected to take; can be completely covered by a 70 mm × 100 mm device. 3). If chronic skin ulcers are present on lower extremities, the skin perfusion pressure must be ³ 30 mmHg at a site proximal or distal to those ulcers. 4). Written informed consent.

Exclusion criteria

1). Have any of the following systemic diseases: uncontrolled diabetes mellitus (defined by HbA1c ³ 10%) according to latest laboratory data obtained within 28 days before registration); requiring continued use of oral corticosteroid therapy (> 20 mg/day prednisolone equivalent); a history of malignant tumor with disease-free interval of 5 years or less. 2). Have a history of allergy to porcine-derived products, collagen, gelatin, bFGF, anesthetic drugs, disinfectants, etc. 3). Have participated in another clinical trial/study within the past three months. 4). Have participated in this study previously. 5). Women meeting any of the following: do not agree to avoid pregnancy during the study; currently pregnant or possibly pregnant; currently breastfeeding. 6). Other patients judged by the investigator or sub-investigator to be inappropriate as a subject of this study.

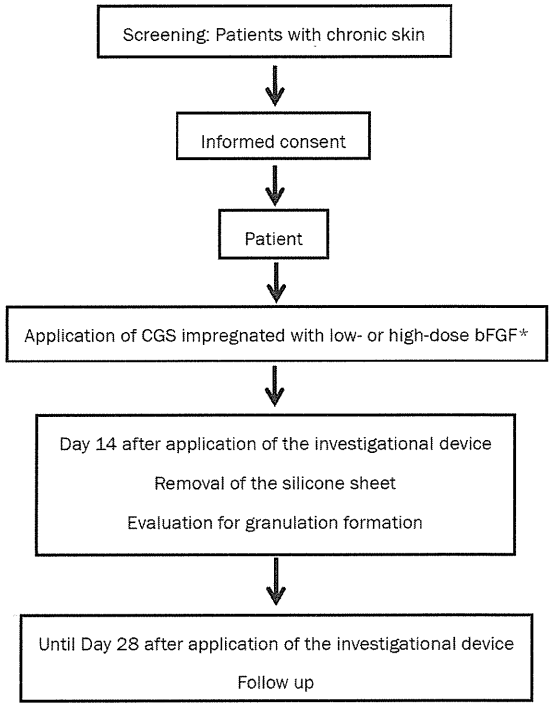

*: Step 1 (non-randomized): low-dose bFGF (n=3): Step 2 (randomized): low-dose bFGF (n=7) and high-dose bFGF (n=7)

Randomization

In Step 2, patients will be randomized to either the low-dose or high-dose bFGF group at a ratio of 1:1 without stratification. Randomization will be performed using a computer-generated random sequence to ensure equal allocation to the two dose groups by a statistician of the independent data center (Department of Clinical Trial Design and Management, Translational Research Center, Kyoto University Hospital).

Interventions

Preparations of CGS impregnated with bFGF

CGS is the modification of conventional bilayered artificial dermis (Pelnac; Gunze Co., Ltd, Kyoto, Japan) and consists of an upper silicone sheet (0.1mm in thickness) and lower sponge (3 mm in thickness) [20]. In this study, the lar-

ger CGS (82 mm × 120 mm) will be used. Two different dose bFGF concentrations of 7 μg/cm^2 (low dose) or 14 μg/cm^2 (high dose) will be used. On the day of study therapy, the investigator or sub-investigator will prepare CGS impregnated with bFGF in the operating room

Application of CGS impregnated with bFGF

This therapy will be started within 28 days of enrollment. After debridement of the chronic skin ulcers, CGS impregnated with bFGF of 7 μg/cm^2 or 14 μg/cm^2 and cut according to the shape of the wound will be applied and sutured to surrounding skin.

Dressing changes and silicone sheet removal

After the application of CGS, dressings will be changed as necessary. Patients will be hospitalized until Day 7 to ensure stabilization of the applied CGS and may be discharged on Day 8 after application according to the condition of the wound. On Day 14 after application, the sutures and silicone sheet of CGS will be removed. After silicone film removal, subsequent therapy may be started.

Subsequent therapy

The use of bFGF or another collagen-based artificial skin will be prohibited until Day 28 after application. The use of ointments, wound dressings and skin grafting will be allowed. After completion of the study period (Day 29 after investigational device application and onward), no particular restrictions will be imposed.

Digital photograph for healing assessment

Using a digital camera, digital images of the wounds will be taken with a calibrator (CASMATCH; BEAR Medic Corp., Tokyo, Japan) placed on the skin adjacent to the wound. The color and size of image will be adjusted using the CASMATCH and image editing software (Adobe Photoshop; Adobe Systems) to assess the wound and granulation areas. As with the primary endpoint, the granulation tissue evaluation committee members will assess the wound and granulation areas.

Primary endpoint

The primary endpoint is "wound bed improvement."

Granulation tissue is wound connective tissue, which forms at the beginning of wound healing [26]. This highly fibrous tissue is usually pink because numerous small capillaries invade granulation tissue to supply oxygen and nutrients. The appearance of granulation tissue is a good sign of healing because when a wound starts granulating, it means that the healing process of the wound is starting [26-28]. The area of granulation tissue will be measured as the granulation formation area in this study. An unhealed area is defined as an area with no epithelialization and no granulation formation. In this study, the percentage of wound bed improvement is defined as the value (%) calculated from the sum of the granulated and epithelialized areas on Day 14 divided by the baseline wound area after debridement on Day 0 multiplied by 100, and the patient is diagnosed with wound bed improvement if the wound bed improvement indicator is 50% or higher. The use of 50% or more as the cutoff for the wound bed improvement indicator is based on the pressure ulcer healing assessment scale by the Japanese Society of Pressure Ulcers [28, 30, 31].

Secondary endpoints

1). Adverse events and adverse reactions. 2). Percentage of "wound bed improvement". 3). Percentage of wound reduction: The percentage of wound area reduction is defined as the value (%) calculated from the wound area of the ulcer on Day 14 divided by the baseline wound area after debridement on Day 0 multiplied by 100. 4). Percentage of granulation area: The percentage of granulation area is defined as the value (%) calculated from the granulation area divided by the wound area on Day 14 multiplied by 100.

Blinding

The baseline wound area, the wound area on Day 14 and the granulation area on Day 14 will be independently measured under blinding by central review. Patients will be unblinded, and unblinded investigators will apply CGSs and change dressings.

Sample size

This study will be conducted to determine whether CGS impregnated with bFGF is promising for the treatment of chronic skin ulcers, as evaluated based on wound bed improvement as

Table 1. Schedule of study assessments and evaluations

	Treatment			Observation
Clinical assessments, testing and investigations	Day of enrollment	Day of application/ reapplication	← →	Day of silicone sheet removal (Day 14)	Day 28 after application/ reapplication
Clinical history	○				
Physical examination	○				
Eligibility criteria check	○				
Informed consent	○				
Blood test	○			○	○
Skin perfusion pressure	○				
Investigational device application		○			
Clinical assessment of the wound	○	○		○	○
Digital photograph of wound	○	○		○	○
Wound evaluation				●	
Data submission of treatment and AE etc.		○		○	○
Observation of AE		○	← ○ →	○	○

○: required; ●: Wound area measurements, granulation area measurements (wound for efficacy evaluation and wounds for study therapy)

the primary endpoint. Primary analyses will be conducted using all data treated with CGS in Step 1 and Step 2. Since debridement and conventional therapies rarely lead to wound bed improvement in this patient population, the null hypothesis tested in this study is that the proportion of patients with wound bed improvement is 10% or less. The null hypothesis is also supported by previous trials [32-34]. In consideration of the minimum clinically important difference, the expected proportion of patients with wound bed improvement in this study is set to 50% or more. When exact testing based on binomial distribution is conducted with a one-sided significance level of 2.5% and a statistical power of 90% or higher, the required number of subjects is 14. Allowing for a drop-out rate of 20% or less, the total number of patients for registration is 17, specifically 3 patients in Step 1 and 14 patients in Step 2.

Study schedule

The schedule of study assessments and evaluations is shown in **Table 1**. The study period will be from the day of informed consent to 28 days after investigational device application. The study period will be from the day of investigational device application to 28 days after investigational device application. Data to evaluate the efficacy and safety of this study will be collected at enrollment, baseline, and Day 14 of the treatment phase and Day 28 of the observation phase.

Statistical analysis

Patients who have been registered for the study and who have undergone investigational device application at least once will be included in the full analysis set (FAS) and the safety analysis

set. From the FAS, however, patients will be excluded if they have serious protocol violations or International Conference on Harmonization Guidelines for Good Clinical Practice (ICH-GCP) violations (failure to obtain consent, major study procedure violations) or if they are found to be ineligible after registration.

Wound bed improvement

Wound bed improvement is the primary endpoint of this study. The primary analysis will be conducted for the FAS using exact test based on binomial distribution with a null proportion of 10% and a one-sided significance level of 2.5%. The 95% confidence interval of the proportion of patients with wound bed improvement will be calculated using an exact method based on binomial distribution.

Percentage of wound bed improvement, would reduction and granulation area

Using the FAS, the descriptive statistics will be calculated. The interval estimation will be conducted under the assumption that this endpoint follows normal distribution.

Adverse events related to the application of the device

Using the safety analysis set, the frequency/incidence of adverse events and adverse events that can be causally related to the investigational device in the safety analysis set will be calculated by event and severity.

Ethical considerations

This study is being conducted in compliance with the ICH-GCP and in agreement with the latest revision of the Declaration of Helsinki, Pharmaceutical Affairs Law and all applicable Japanese laws and regulations, as well as any local laws and regulations and all applicable guidelines. This protocol and any amendments have Institutional Review Board approval at Kyoto University Hospital.

Subject consent

Informed consent will be obtained from all potential study participants using the IRB-approved informed consent form. The clinical investigator informs the potential study subject of all pertinent aspects of the study. The subject must sufficiently understand the contents of the information form before providing written consent. The consent form must be dated and signed by both the investigator and the participant. Subjects are also informed that their medical care will not be affected if they do not choose to participate in this study. The consent form will be retained at Kyoto University Hospital and the information form and a copy of the consent form will be handed to the participant. Whenever the investigator obtains information that may affect the participant's willingness to continue participation in the study, the investigator or sub-investigator will immediately inform the participant and record this, and reconfirm the participant's willingness to continue participation in the study.

Adverse events

This study is being conducted according to the ICH-GCP. Adverse events and serious adverse events information will be documented according to the Medical Dictionary for Regulatory Activities (MedDRA) version 14.0.

Results and discussion

This study has been designed to address the safety and efficacy of novel treatment for chronic skin ulcers using a modified artificial dermis, CGS, that can sustain bFGF. This study will be the first randomized controlled trial to evaluate the efficacy of CGS and the appropriate concentration of bFGF impregnation for treatment of increasing non-healing ulcers. Some bioengineered skin substitutes that provide growth factors secreted by living cells have been reported to be effective for chronic skin ulcers, although they are costly and access is limited to only a few areas and countries. Both CGS and bFGF are freeze-dried and can be kept well and stored at room temperature. These are off-the-shelf products and the procedure of impregnation is simple; therefore, we can use this combination therapy anywhere when needed. If successful, this intervention may lead to substantial and important changes in the management of chronic skin ulcers, such as diabetes ulcers and venous leg ulcers

Acknowledgements

This work was supported by a grant from the